Journal of Water Process Engineering 52 (2023) 103549

Contents lists available at ScienceDirect

Journal of Water Process Engineering

journal homepage: www.elsevier.com/locate/jwpe

Highly efficient $Cu_2O@Cu_xFe_yO_4$ nanohybrid catalyst for the degradation of emerging pollutants

S. Fernández-Velayos [a], F.J. Recio [a], F.J. Palomares [b], N. Menéndez [a], P. Herrasti [a], E. Mazarío [a,*]

[a] Departamento de Química Física Aplicada, Facultad de Ciencias, Universidad Autónoma de Madrid, C/Francisco Tomás y Valiente, 7, Cantoblanco, 28049 Madrid, Spain
[b] Instituto de Ciencia de Materiales de Madrid (ICMM), A.E. Consejo Superior de Investigaciones Científicas (CSIC), 28049 Madrid, Spain

ARTICLE INFO

Keywords:
Advanced oxidation process
Sodium persulphate
Catalyst
Degradation
Tetracycline
Emerging pollutants

ABSTRACT

$Cu_2O@Cu_xFe_yO_4$ nanohybrids (NHs) have been electrosynthesized by a simple and environmentally safe method to be used as catalysts for tetracycline degradation. NHs shown an average diameter of 14(5) nm and exhibit high crystallinity with spherical morphology. XPS results demonstrate a cuprite-enriched surface; meanwhile, the inner layer is composed by a nonstoichiometric copper spinel structure. The degradation has been monitored by UV–Visible spectroscopy, TOC analysis, and HPLC. The electrochemical characterization demonstrates the synergetic effect of Fe^{3+}/Fe^{2+} and Cu^{2+}/Cu^{+} coupling to enhance the activation of persulfate. This effect results in a greater degradation efficiency of NHs than other catalysts, namely, Cu_xO_y, Fe_3O_4, and a mixture of both and Cu_2O.

It has been found that a previous adsorption stage before degradation does not improve the elimination of the pollutant and its length in time, with a TOC reduction of 72.6 % in 2 h. Conversely, conducting the oxidative process in a direct step resulted in a more rapid and efficient process, 82.3 % of reduction in 1 h. Through this method, the catalyst reutilization resulting in a decrease of 50 % in TOC degradation from the third use, while the TCY concentration degraded remains almost constant. This reduced catalytic activity with use might be a consequence of 1) the absence of the single Cu-oxide layer due to the leaching of mainly Cu ions but also Fe ions during the degradation tests, and, 2) the passivation of the outermost layer, mainly covered by C—O species and OH groups, which hinders access to active catalyst sites.

1. Introduction

Tetracyclines (TCs) are a group of widely used antibiotics, including tetracycline (TCY), chlorotetracycline (CTC) and oxytetracycline (OTC). These compounds are used as treatment for bacterial infectious diseases in humans and animals, and as alimentary supplements to improve livestock growth [1,2]. TCs degradation is very challenging for human and animal metabolisms, which causes the excretion through urine and feces of around 70 % of the TCs administrated. After their excretion, TCs end up in soils and wastewater, causing their contamination [2].

Wastewater treatment plants get rid of a small amount of the antibiotics in wastewater, and another significant part is released into the medium [2]. Several studies have been conducted to determine the impact of TCs on the environment, showing their toxicity for some aquatic species [3,4]. Moreover, the presence of TCs in wastewater promotes the increase of antibiotic-resistant genes in some microorganisms, which can be a significant problem for human health when these microorganisms are present in drinking or irrigation water [2,5–7]. Thus, it is necessary to find new efficient methods to remove TCs compounds from the soils and wastewater.

Advanced oxidation processes (AOPs) are an excellent way to degrade and mineralize organic pollutants in wastewater, due to its unique advantages including ease of operation, high degradation efficiency and benign process. AOPs are based on the in-situ generation of radicals that oxidize the organic compounds causing their transformation into smaller molecules and even CO_2 and H_2O [8,9]. The most common radicals used in these processes are hydroxyl radicals ($^{\bullet}OH$), produced through the activation of hydrogen peroxide (H_2O_2), and sulphate radicals ($SO_4^{\bullet-}$), which can be generated by oxidants like persulfate ($S_2O_8^{2-}$). In the last years, sulphate radicals drew a lot of attention because they have a higher redox potential ($E_0(SO_4^{\bullet-}/SO_4^{2-})$ = 2.60–3.10 V vs NHE) than the hydroxyl ones ($E_0(^{\bullet}OH/OH^{-})$ =

* Corresponding author.
E-mail address: eva.mazario@uam.es (E. Mazarío).

https://doi.org/10.1016/j.jwpe.2023.103549
Received 7 November 2022; Received in revised form 3 January 2023; Accepted 29 January 2023
Available online 7 February 2023

1.90–2.70 V vs NHE) [10]. Also, persulfate is more stable than hydrogen peroxide and can be transported for a longer time before being activate for the pollutants degradation [11]. Homogenous, or heterogeneous catalysts are the most studied method for persulfate activation. Furthermore, heterogeneous AOPs sometimes are combined with other sources of energy to improve antibiotics removal from wastewater such as ultrasounds, electricity [12] or UV [13–16]. The use of a mixture of persulfate anions and homogeneous ferrous cations in acidic media has been studied in AOPs [17,18]. Nevertheless, some problems arise: (i) the catalyst cannot easily be recovered after its use, and (ii) the processes require very low pH (~3) that has to be neutralize after process generating iron residues. Hence, new investigations are focused on the development of heterogeneous catalysts, which can be recovered and used several times [17]. Many researchers have focused their attention on bimetallic and trimetallic catalyst [19,20], being the formation of $SO_4^{\bullet-}$ via transition-metal catalysis the main oxidizing specie [21,22]. Minxian et al. has reported the tetracycline degradation mechanism with a catalyst obtained from Fe sludge doped with Cu ions. They reported the benefits of the synergic redox couple Cu^{2+}/Cu^{+} ($E^{\circ} = 0.17$ V) and Fe^{3+}/Fe^{2+} ($E^{\circ} = 0.77$ V) in the persulfate activation [23]. The possible degradation mechanism in a bimetallic catalyst consists of Fe and Cu transition metal was proposed as follow: Fe^{3+} react with persulfate to form Fe^{2+} and $S_2O_8^{\bullet-}$ radicals, the Fe^{2+} activate persulfate ions to form active sulphate radicals (Eqs. 1–2), the same reaction also take place with Cu^{2+} and Cu^{+} species (Eqs. 3–4). In addition, the standard reduction potentials of Fe and Cu species creates a conductive atmosphere for the reduction of Fe^{3+} to Fe^{2+} and Cu^{+} to Cu^{2+} (Eq. 5) [24]. Moreover, $OH^{\bullet}$ is generated but has a minor contribution in the degradation process (Eq. 6). Finally, the degradation mechanism showed that TCY could be partially or totally removed because of $SO_4^{\bullet-}$ and $OH^{\bullet}$ (Eq. 7).

$$Fe^{3+} + S_2O_8^{2-} \rightarrow Fe^{2+} + S_2O_8^{\bullet-} \quad (1)$$

$$Fe^{2+} + S_2O_8^{2-} \rightarrow Fe^{3+} + SO_4^{2-} + SO_4^{\bullet-} \quad (2)$$

$$Cu^{2+} + S_2O_8^{2-} \rightarrow Cu^{+} + S_2O_8^{\bullet-} \quad (3)$$

$$Cu^{+} + S_2O_8^{2-} \rightarrow Cu^{2+} + SO_4^{\bullet-} + SO_4^{2-} \quad (4)$$

$$Fe^{3+} + Cu^{+} \rightarrow Fe^{2+} + Cu^{2+} \quad (5)$$

$$SO_4^{\bullet-} + H_2O \rightarrow OH^{\bullet} + SO_4^{2-} + H^{+} \quad (6)$$

$$OH^{\bullet} + SO_4^{\bullet-} + TCY \rightarrow Intermediate + H_2O + CO_2 \quad (7)$$

More recent studies about TCY degradation by heterogeneous AOPs using Cu and Fe as the main catalyst components are presented in Table 1. In some of these works, ferrites nanoparticles are supported by other materials to improve the degradation efficiency.

In the light of all we have mentioned, the present study was focused on the one-step electrochemical synthesis and characterization of NHs constituted by $Cu_2O@Cu_xFe_yO_4$ nanoparticles, and their application as catalysts in TCY degradation via persulphate activation. Moreover, the proposed green methodology for the NHs synthesis can be scaled up easily, as has been already demonstrated by previous research in magnetite, producing about 1 g of catalyst hourly [30]. The catalytic activity of the catalyst will be compared with different catalyst constituted by only iron (Fe_3O_4), only copper (Cu_2O) and a mixture of both. In addition, the competing relationship of the adsorption/degradation processes on the final catalytic efficiency is demonstrated. Finally, the catalyst reusability is also proposed.

2. Experimental part

2.1. Catalysts synthesis

The synthesis of $Cu_2O@Cu_xFe_yO_4$ nanohybrids (NHs) was performed following a similar protocol published by our group for the electrosynthesis of cobalt ferrite nanoparticles [31]. Briefly, two foils of iron and copper of 2 cm^2 each, were used as anode electrodes, and a cylindrical cathode of iron was placed around those electrodes whose area was 120 cm^2. The use of a larger cathode surface placed around anode electrodes ensure a homogeneous current distribution. Current densities of 50 mA/cm^2 were applied to iron and copper foils to promote the oxidation and release of copper and iron cations through the solution. At the same time, in the cathode, the water reduction takes place and generates hydroxyl species, which produces a basic pH in the solution. At this pH, the generation of copper and iron oxides is favoured. 0.04 M of NaCl aqueous solution was used as a supporting electrolyte. The synthesis temperature was controlled by a thermostat bath at 25 °C. The solution was magnetically stirred at 1100 rpm during 30 min of reaction. A scheme of the reactor is provided in Fig. 1. In the first stages of the electrochemical synthesis, the solution turns black, remaining unchanged until the end of the reaction period. Afterward, the NHs were separated from the electrolyte solution with a magnet and washed three times with distilled water, following the sequence, sonication for 5 min, and magnetic decantation until the supernatant was clear. The washed NHs were dried under vacuum at room temperature.

To compare the degradation efficiency of the nanohybrids, magnetite nanoparticles were synthesized following the electrochemical method in

Table 1
Recent studies of TCY degradation with catalyst consist of Fe and Cu elements.[a]

Catalyst	Reaction time (min)	Catalyst dose (g/L)	Oxidant (mM)	TCY (ppm)	pH	T (°C)	TCY rem (%)	TOC removal (%)	Ref
$AC@Fe_3O_4$	180	0.4	PS 40	10	3	25	99.8	50.7	[17]
Fe_3O_4	120	0.24	H_2O_2 20	60	7.4	25	98	–	[25]
Fe_3O_4-Cs	120	0.5	H_2O_2 10	48.09	3.0	25	96.2	68.3	[26]
$Cu/CuFe_2O_4$	120	0.3	PS 7.8	50	3.5	25	75	60	[27]
CuO@C-550	60	0.2	PMS 1.0	20	6	28	≈100 (HPLC)	75.3	[28]
$Cu_2O@Cu_xFe_yO_4$	60	1	PS 0.5	100	6	25	98.1	82.3	This work
Process assisted by ultrasounds									
Fe_3O_4	60	1.0	H_2O_2 150	100	3.7	22	93.6	31.8	[13]
Process assisted by electricity									
Fe_3O_4	60	0.2	PS 2.0	25	4.5	25	86.53	–	[15]
Process assisted by ultraviolet light									
Fe_3O_4	120	0.3	H_2O_2 10	50	7.0	25	97.5	56.5	[29]

[a] PS is persulphate, H_2O_2 is hydrogen peroxide, HPLC is high performance liquid chromatography, PMS is peroxymonosulphate, TOC removal, is total organic content removal.

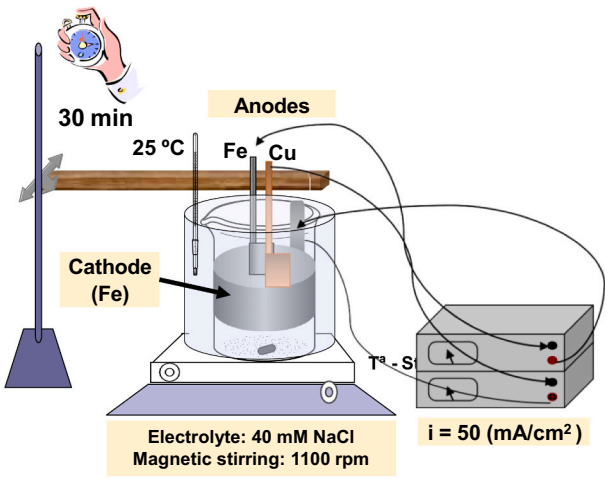

Fig. 1. Scheme of the electrochemical synthesis of NHs.

a mixture of 20:80 methanol:water previously reported by our group [32]. In this case, only a foil of iron acts as the anode, while the cathode is parallel to the anode electrode. With this methodology, we were able to synthesize magnetite nanoparticles (NPs) with similar size to those of NHs.

At the same time, the electrochemical methodology was used to synthetized copper oxide catalyst (Cu_xO_y), following the same protocol described for NHs synthesis, but using a single copper electrode as anode.

2.2. Catalyst characterization

The morphology of the NHs were evaluated by High Resolution Transmission Electron Microscopy (HRTEM) using a Tecnai F30 (FEI) electron microscope operated at 300 kV. Also, a JEOL-2000 FXII (TEM) electron microscope operating at 120 keV was used to routinary visualize the morphology of the catalysts and obtain the size distribution. The leaching of copper and iron in the reusability runs from the catalysts, and the metal content in the fresh and four times used NHs, were determined with a Plasma Emission Spectrometer ICP-OES Perkin Elmer mod. Optima 2100 DV. Catalyst phase identification was examined by X-ray diffraction (XRD). The diffractograms were collected on Bruker D8 powder diffractometer equipped with a primary monochromator and an ultrafast Lynxeye XE-T multichannel detector with Cu $K_{\alpha 1}$ radiation. PANalytical X'Pert HighScore software [33] was used for data analyses and Full Proof Suit package [34] was used to quantify the percentage of the catalyst crystalline phases.

X-ray photoelectron spectroscopy (XPS) has been used to characterize the elemental composition and the oxidation states of Cu and Fe on the surface of the NHs samples. XPS experiments were performed using an X-ray source of Al-Kα (1486.6 eV) [35]. The spectra were analyzed with the CasaXPS program (Casa Software Ltd., Cheshire, UK) using a Shirley method for background subtraction and data processing for quantitative XPS analysis. Spectra are displayed after subtracting the contribution of the Al-Kα satellite emission; in some cases, the spectra were normalized to the maximum intensity to highlight line shape differences, which provides direct valuable insight regarding the oxidation states.

2.3. Electrochemical tests

The electrochemical characterization of the active species on the NHs surface was performed in a conventional electrochemical cell. Glassy carbon electrodes (GC) of Area = 0.196 cm^2were used as working electrodes. The electrode was pre-cleaned through polishing with alumina powder (0.3 and 0.05 μm consecutively), and then washed with Milli-Q water. To modify the electrode surfaces, a catalytic inks were prepared dispersing 1 mg of the catalyst and 4 mg of carbon Vulcan XC-72R in 5 mL of isopropanol:water (1:4 v/v) and 20 μL of Nafion, under sonication for 30 min. The electrodes were modified by spin coating dropping 20 μL of the catalytic ink on the GC surface. The electrochemical analyses were performed using an Autolab 302 N potentiostat and a Pine Rotation Rate Control Unit. Graphite rod and Ag/AgCl electrode were used as counter and reference electrode, respectively. The potential values have been referred to reversible hydrogen electrode (RHE) using the relation: E(RHE) = E(Ag/AgCl) + 0.199 + 0.059 pH. Electrochemical characterization was performed by cyclic voltammetry at pH 6, in N_2-saturated solutions. The electrocatalytic tests were performed with a rotating electrode at 1600 rpm at pH 6 in N_2 saturated solutions and in presence of 0.5 mM of sodium persulphate (SPS).

2.4. Adsorption and advanced oxidation process (AOPs)

Adsorption process, the adsorption evaluation process was performed for 2 h under mechanical agitation (680 rpm), in a thermostatic bath at 25 °C. In a typical experiment, 1.0 g/L of NHs was dispersed in a TCY aqueous solution (25 mL) at pH 6 of 100 ppm. Two conventional kinetic models, pseudo-first-order ($q_t = q_e(1 - e^{k_1 t})$) and pseudo-second-order ($q_t = q_e^2 k_2 t/1 + q_t k_2 t$), were applied to investigate the adsorption kinetic further. Advance oxidation process (one step protocol), the experimental conditions were the same as described for adsorption process, but for this experiment, 0.5 mM of SPS was added to the TCY solution before adding the catalyst. The performance of the different catalyst on the degradation reaction of TCY were studied with this protocol. The reusability of the NHs was evaluated by performing four cycling runs. After the completion of the reaction, the separated NHs were washed with distilled water and dried for the subsequent cycle test. Advance oxidation process (two steps protocol), a mixture of the two previous protocols were conducted. At the same adsorption conditions, the catalyst was in contact with the pollutant for 1 h to ensure a steady state equilibrium. Afterward, 0.5 mM of SPS was added into the above mixing solution and immediately the degradation begins, and last 1 h.

Pollutant elimination quantification, at the given time, sample aliquots (1.0 mL) were withdrawn from the test and centrifuged for 2 min at 12,000 rpm. Those samples were analyzed by monitoring the absorbance at λ_{max} = 357 nm in UV–Vis spectra with a Perkin Elmer UV Vis Lambda 365 spectrophotometer. The quantification of the total organic content (TOC) left in solution with time last 1 h, was analyzed with a TOC-5000A model Shimadzu analyzer, considering the average of at least three measurements with an accuracy of ±5 %. The evolution of tetracycline concentration was also analyzed by ultra-high performance liquid chromatography (UHPLC/MSMS) (EVOQ-ELITE) using an Ace Excel 2 column (100 mm length, 3 mm diameter) as stationary phase. Analyses were performed using a mixture of H_2OmQ + 0.5 % formic acid and methanol + 0.05 % formic acid as mobile phase with a proportion 98/2 % (v/v).

3. Results and discussion

3.1. Nanohybrids characterization

TEM image of NHs shown in Fig. 2a presents nanoparticles with quasi spherical morphology with a mean diameter of 14(5) nm. The synthetized NHs presents high crystallinity reflected in the clearly visible crystallographic planes observed in the high-resolution TEM image, Fig. 2b.

The metal analysis obtained by ICP in the NHs reveals an important amount of copper with a total Fe/Cu molar ratio of 2.66. XRD pattern of fresh NHs sample depicted in Fig. 3, presents broad reflexions correlated with particles in the nanosized regimen. The analysis of the obtained pattern reveals two structures, attributed to cubic spinel (MFe_2O_4, with M = Cu, Fe) and cuprite (Cu_2O) structures with space group Fd-3m:227

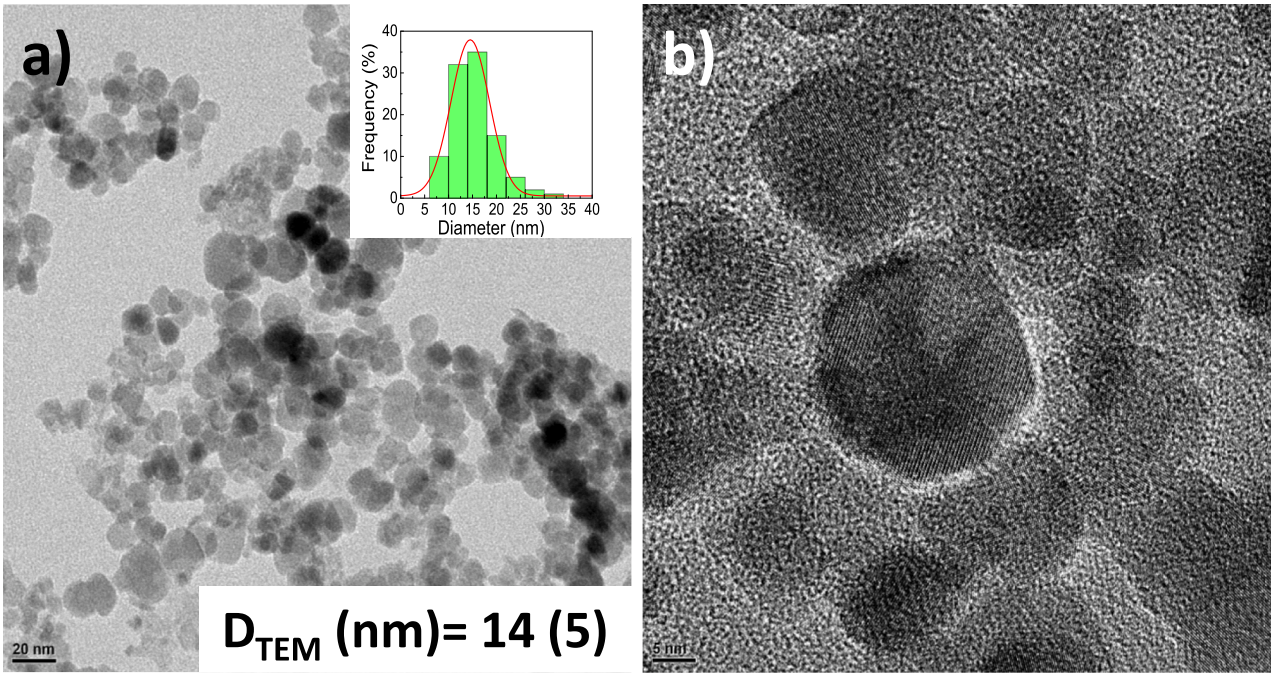

Fig. 2. a) TEM images of fresh NHs electrochemically synthetized; inset histogram analysis of the nanoparticles size. b) HRTEM image of a few dispersed NHs.

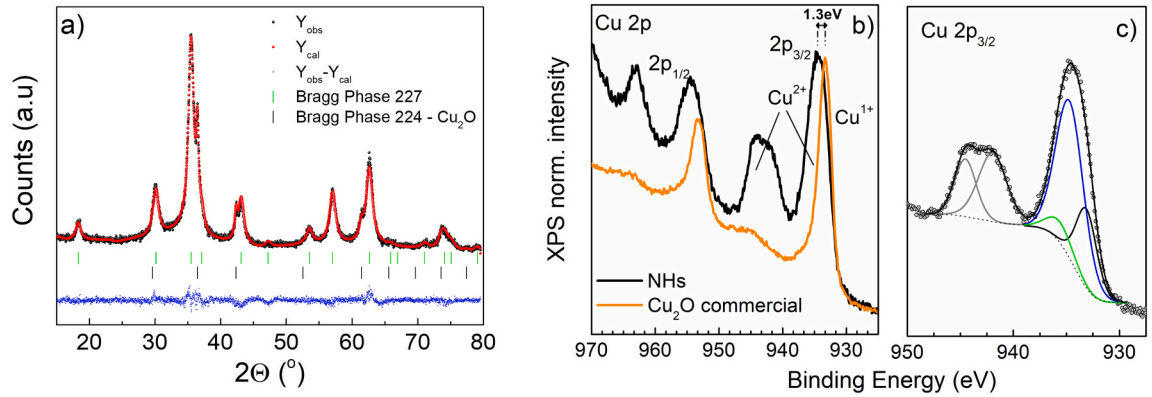

Fig. 3. a) XRD Rietveld analysis of pattern NHs. Phase: 1 — (227), Bragg R-factor: 2.56, $R_{f\text{-}factor} = 1.42$. Phase: 2 — Cu_2O (224) Bragg R-factor: 3.21, $R_{f\text{-}factor} = 3.43$. $\sigma^2 = 0.981$. (Bragg positions are depicted in green for spinel structure and black for Cu_2O). b) XPS spectra of the Cu 2p corresponding to NHs and commercial Cu_2O samples. XPS spectra were normalized to maximum peak intensity. Emission from Cu^{1+} and Cu^{2+} oxidation states and line shape differences are tagged. c) XPS spectra of the Cu $2p_{3/2}$ corresponding to NHs together with fit resulted from the addition of chemically shifted and satellite components ascribed to different oxidation states. Data points are represented as open symbols, and Shirley background and components as dotted and solid lines, respectively. Cu^{1+} (black), Cu^{2+}: CuO (blue) and $Cu(OH)_2$ (green). (For interpretation of the references to colour in this figure legend, the reader is referred to the web version of this article.)

and Pn-3m:224, respectively. The lattice parameter analysis of the cubic spinel is 8.383(1) Å. This value is in the range of other cooper ferrites, 8.424–8.3715 Å, synthesized by coprecipitation method followed by calcination at different temperatures [36,37], and higher than the lattice parameters reported for electrosynthetized iron ferrite nanoparticles described in bibliography with similar particle sizes (8.370–8.374 Å) [32], which is associated to the bigger Cu^{2+} atomic radius when compared to Fe^{2+} one.

It is worth to mention that in nanosized regime maghemite (Υ-Fe_2O_3), magnetite (Fe_3O_4), copper ferrite ($CuFe_2O_4$) and copper-doped iron oxide have cubic spinel structures at room temperature [36,38] with similar lattice parameters, which makes it difficult to ensure the NHs composition. Seeking to clarify this point, detailed XPS analysis is further performed in the fresh NHs, to get some insight on the iron and copper oxidation states.

The overall atomic concentration (% at.) surface composition of the NHs sample was summarized in Table S1. The Cu/Fe ratio obtained for the 3p and 2p levels reports values corresponding to a higher Cu content than that calculated from the ICP analysis, which determines the composition of the whole NHs molar ratio. In addition, the Cu/Fe ratio for the 2p level also provides a significantly higher and very distinct value than that obtained for the 3p state. 2p peaks provide surface sensitivity since their emission comes mostly from the outermost layers of the NHs. On the contrary, low binding energy signals from 3p levels with higher kinetic energy are emitted from deeper regions, which significantly enhances the contribution from the NHs as a whole, with minor influence from the outer surface layers. These results indicate the enrichment of copper atoms on the surface of the NHs. A detailed line shape analysis of XPS spectra is required to obtain information on the oxidation state of copper. Fig. 3b compares the normalized Cu $2p_{3/2}$ spectra corresponding to NHs with the representative signal from commercial Cu_2O. The first thing to be noticed in the commercial reference

sample is the absence of satellite emission at binding energy in the range from 940 to 945 (Cu $2p_{3/2}$) and 960 to 965 eV (Cu $2p_{1/2}$) respectively, whose are known to be characteristic of the CuO phase [39,40]. In contrast, there is a relative shift towards lower binding energy of ca. 1.3 eV in the peak position of the Cu_2O commercial sample with respect to NHs one. This peak appears at the binding energy position of the shoulder seen on the right side of the Cu $2p_{3/2}$ emission for the NHs sample and can be inferred to Cu^{1+} oxidation state.

Peak fitting of the Cu $2p_{3/2}$ spectra (Fig. 3c) was done by using the deconvolution of the component obtained from the fit of the Cu_2O reference [39,40] and several mixed Gaussian/Lorentzian symmetric functions for Cu^{2+} oxidation state and satellites components, using as parameters the binding energy shifts reported in [39]. The first result is that copper is fully oxidized, mostly as CuO, but XPS also allows distinguishing some contribution from Cu_2O and $Cu(OH)_2$.

Let us turn our attention to the Fe region (Fig. S1). The described analysis (see discussion in SI) suggests that Fe^{3+} mostly forms the Fe oxide signal in the NHs samples, even though the presence of Fe^{2+} species cannot be discarded, in good agreement with the formation of Cu-doped iron ferrite nanoparticles. Based on these results, the Rietveld analysis of the fresh NHs present a core with an 88.3 % of $Cu_{0.34}Fe_{2.66}O_4$ (where a partial substitution of the Fe^{2+} sites by Cu^{2+} takes place) and the outer layers of the catalysts with 11.7 % of Cu_2O, which perfectly agrees with the Fe/Cu molar ratio obtained by ICP.

3.2. Catalytic evaluation

3.2.1. The degradation performance of TCY

Before the AOPs experiment of Tetracycline, the adsorption of the as-prepared NHs to the target compound was conducted. The TCY is an amphoteric molecule symbolized as $TCYH_2$ with multiple ionizable functional groups at different pHs. $TCYH_3^+$ is the predominant specie at pH < 3.3, $TCYH_2$ specie is predominant in the range 3.3 < pH < 7.7, while anionic $TCYH^-$ is predominant specie for pHs at 7.7 < pH < 9.7, and finally, TCY^{2-} is stable at pH > 9.7 [41,42]. Two conventional kinetic models, pseudo-first order and pseudo-second order, were applied to investigate the adsorption kinetic further. The kinetics parameters obtained from the two models are listed in Table S2 and the fitting graph is depicted in Fig. S2. The R^2 value (>0.96) of the fit according to the pseudo-second-order rate model was higher than the obtained from the pseudo-first-order rate model ($R^2 = 0.921$). In addition, the values of $q_{e,cal}$ derived from the pseudo-second-order rate model fit was closer to the $q_{e,exp}$ values. Accordingly, the pseudo-second-order kinetic model better represents the adsorption of TCY onto NHs [43]. The adsorption removal efficiency obtained following the decrease in the maximum on the visible spectrum (Fig. 4a) is about 60 % with a $q_{e,cal}$ value of 66 mg/g, in agreement with the 59 % removal after 1 h determined by TOC and with the 43.7 ppm of antibiotic left in the supernatant, measured by HPLC for the same experiment, Fig. 4a and b. The NHs Point of Zero Charge (PZC) is around pH 7, Fig. S3. So, the surface of the catalyst was negatively charged at working pH, and the dominant TCY species is $TCYH_2$, hence, the poor electrostatic repulsion experienced at this pH results in the high adsorption capacity observed. In addition, the interaction of Cu^{2+} with oxygen atoms of TCY molecules enhance the adsorption efficiency of the pollutant [44]. In another experiment, the pollutant and the catalyst were mixed up to reach the adsorption equilibrium, afterwards, the AOPs started with adding 0.5 mM of SPS and lasted 1 h, Fig. 4a and b. First, is worthy to mention that without catalysts, only SPS cannot degrade Tetracycline, although persulphate anion ($S_2O_8^{2-}$) has a high oxidation potential ($E_0 = 2.01$ eV), its kinetically slow in reacting with many organic compounds [45]. However, when the catalyst is involved in the reaction, a very fast catalytic degradation of TCY is observed in the early instants of the reaction, caused by the chemical activation of the persulfate anion to generate the intermediate sulfate free radical oxidant ($SO_4^{\bullet -}$, $E_0 = 2.6$ V) [46]. We have also compared the degradation efficiency obtained with no previous adsorption stage against the experiment conducted in separate stages, first adsorption and later degradation. The TOC removal and TCY left in solution of those experiments are represented in Fig. 4b. Targeted pollutant left in solution after only degradation and adsorption + degradation processes is very similar, with values of 1.95 and 1.0 ppm, respectively. A good elimination performance of TCY is important, but even more crucial is the mineralization percentage measured by TOC, since it measures not only the amount of degraded TCY, but also the by-products of the oxidation reaction. In this sense, the TOC mineralization efficiency is slightly lower in the two steps protocol (72.6 %) than in the direct degradation reaction (82.3 %). This variation in the TOC obtained can be explained with the high adsorption capacity of Cu^{2+} to bind with the TCY, which limits the further degradation process by hiding the catalyst's active sites in the two steps experiment. Similar results were observed for the degradation of TCY with a porous Fe_3O_4 catalyst embedded in chitosan as the pollutant concentration increased [26] and with CuO particles encapsulated in a carbon framework [28].

In other words, the adsorption process is kinetically uncompetitive with the degradation process, since, once the one step oxidation starts, the decolorization/degradation happens within the first minutes, lowering the C/Co of the pollutant ratio from 1 to nearly 0.2, representing an 80 % decrease in the targeted pollutant content within the first few minutes. Furthermore, in the two-step method, the larger experiment time could compromise the reusability of the catalyst in further cycles by the possible leaching of Fe and Cu cations. We can conclude that the one-step protocol is time-saving and conducted to greater degradation doses.

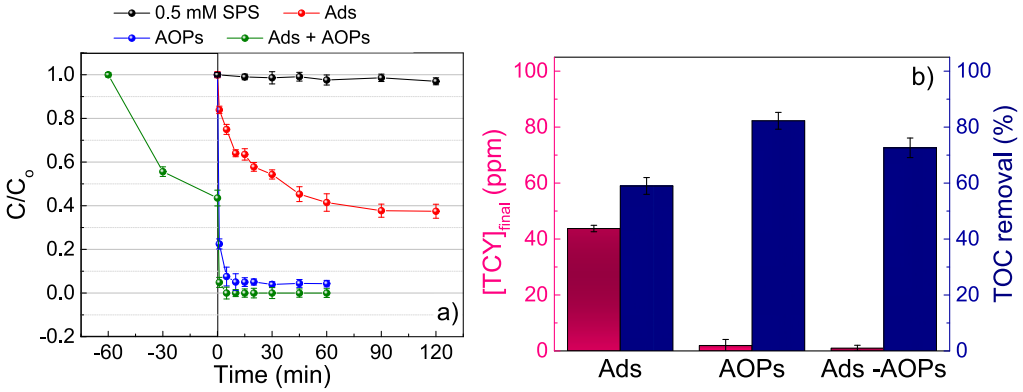

Fig. 4. a) UV–Vis spectral changes for TCY degradation with NHs in one step (adsorption or AOPs) and two steps experiment (adsorption + AOPs). b) Target TCY concentration left measured by HPLC and TOC removal percentage for 1 h of experience. Unless otherwise stated, the reaction conditions are based on: [TCY] = 100 ppm, [catalyst] = 1.0 g/L, T = 25 °C, [SPS] = 0.5 mM and pH = 6.

3.2.2. Electrochemical catalytic evaluation of NHs vs Fe_3O_4

As we have already explained, the NHs composition is 88.3 % of Cu-doped ferrite and 11.7 % of cuprite. To assess the role of the Fe^{3+}/Fe^{2+} and Cu^{2+}/Cu^{+} on the NHs composition and for comparison purposes we have performed the AOPs with Fe_3O_4 and NHs under the same experimental conditions. The decolourisation test and the TOC removal shown a great difference between those, reaching with the NHs a complete decolourisation in the first 10 min, while the Fe_3O_4 remain around 0.8 throughout the course of the experiment, Fig. 5. Besides, the TOC removal values were 82 and 8 % for NHs and Fe_3O_4, respectively.

To characterize the superficial active sites contribution in the activation of SPS in the degradation test, an electrochemical characterization was performed by cyclic voltammetry with the NHs and Fe_3O_4 nanoparticles (scan rate: 5 m V/s, at pH 6 in N_2 saturated solutions). Fig. 6a shows the voltammograms recorded for both catalysts. As can be observed, the Fe_3O_4 nanoparticles show an irreversible faradaic process ($E_a = 0.42$ V, $E_c = 0.24$ V vs. RHE) which corresponds to the Fe^{3+}/Fe^{2+} redox process of the superficial iron of the nanoparticles [47]. However, the voltammogram for the NHs presents an extra reversible process at more positive values ($E_a = 0.65$ V, $E_c = 0.58$ V vs. RHE) which is associated to the Cu^{2+}/Cu^{+} redox process of the copper atoms present in the NHs. In addition, the cathodic peak of the Fe^{3+}/Fe^{2+} process is shifted to more positive values compared with the magnetite nanoparticles ($E_c = 0.38$ V vs. RHE). This displacement could be associated by the presence of cooper in the NHs structure, which can induce an electron-withdrawing effect on the iron atoms and consequently shift the reduction process to more positive values. To elucidate whether the iron or copper in the structure is responsible for the SPS activation, electrocatalytic tests were performed by rotating disc electrode (RDE) (1600 rpm) in the presence of 0.5 mM of SPS at pH 6. The solution was previously de-oxygenated with N_2 to avoid the presence of O_2 in the solution and hinder the oxygen reduction reaction via $2e^-$ with the consequent generation of H_2O_2, which could interfere in the electrocatalytic reduction of SPS. Fig. 6b shows the polarization curves recorded. The electrocatalytic activity was evaluated considering the onset potential of the SPS reduction (potential when the SPS reduction takes place). The electroreduction of SPS for both catalysts presents different onset potentials, at 0.57 V and 0.30 V vs. RHE for the NHs and Fe_3O_4 NPs, respectively. This fact informs the higher electrocatalytic activity of the NHs than the Fe_3O_4, due to the lower overpotential needed to start the electroreduction. Additionally, the onset potential of the electroreduction of SPS is related to the redox processes Fe^{3+}/Fe^{2+}or Cu^{2+}/Cu^{+} determined by cyclic voltammetry for Fe_3O_4 and NHs, respectively. That is, the electroreduction of SPS starts with the presence of Cu^{+} of the NHs or the presence of Fe^{2+} in the Fe_3O_4 nanoparticles, in which both sites are electrogenerated during the cathodic polarization [48].

3.2.3. Catalytic performance of NHs compared to other catalysts

To further understand the catalytic abilities of the NHs proposed, and the role of the Cu^{2+}/Cu^{+} and Fe^{3+}/Fe^{2+} redox couples, we have also assessed the catalysis efficiency of a commercial cuprite compound where only Cu^{+} is present in the sample. These tests have been performed for three distinct cuprite concentrations, i.e. 0.3, 1.0 g/L and 0.117 g/L, the final concentration found in the NHs sample. The TOC degradation percentages are shown in Fig. 7a. With increasing the catalyst concentration, an increment in TOC degradation has been observed, achieving 18, 36 and 64 % of mineralization with the dose increase, all these values are lower than that obtained by using the NHs catalyst (1.0 g/L). Otherwise, the carbon degradation observed using the same dose (0.117 g/L) of cuprite that the NHs is supposed to have, is about 18 %, far from the value obtained for the nanohybrid (82 %), also with the maximum dose of cuprite catalyst (1.0 g/L) the TCY removal is lower. This implies that not only the Cu^{+} ion is involved in the degradation process, but also the contribution of Cu^{2+}, Fe^{2+}, and Fe^{3+} cations are of key importance.

To provide a more realistic comparison of the TCY degradation obtained with the NHs, we followed a similar experimental method described for the NHs synthesis, but a single copper foil was oxidized in the electrolyte solution. The Cu_xO_y catalyst obtained were composed of quasi-spherical particle aggregates and rod shape morphology, as shown in Fig. S4. The Rietveld analysis of the XRD pattern shows four well-differentiated phases of Cu_2O, CuO, and $Cu(OH)_2$ as well as Cu in a residual proportion which were not able to be separated in the washing processes, Fig. S5. Therefore, the sample we refer to as Cu_xO_y is composed of both Cu^{2+} and Cu^{+}.

The catalytic activity of Cu_xO_y (1.0 g/L) and NHs (1.0 g/L) catalyst was compared with the one obtained with a mixture of Cu_xO_y and spinel iron oxide powders in the same NHs proportion provided by Rietveld analysis (11.7:88.3), in order to have Cu^{2+}/Cu^{+} and Fe^{3+}/Fe^{2+} contributions, Fig. 7b, c. Even if the concentration of TCY left in the solution following the degradation is comparable for both NHs and the mixed sample catalysts, the total organic removal is notably greater for the former catalyst. This demonstrates that there might be a synergistic effect in the hybrid by the presence of copper ferrite, thereby enhancing the relative rates of mass transfer to reactive sites and chemical reaction on these.

3.2.4. The stability and application in various runs

The catalyst recycling performance is of importance in real-world application. Hence, the catalyst was recovered to perform several runs further to investigate the catalytic stability of the NHs in AOPs. Fig. 8a, depicts the UV visible color removal of NHs in the four runs explored. A greater decrease in the C/Co ratio is observed mainly from the third cycle and onwards. The HPLC analysis of TCY removal is shown in Fig. 8b, the concentration of degraded TCY was 98.1, 96.6, 95.1 and 90.9 ppm, in the four sequential runs. In the TOC analysis, we found the most significant differences between cycles. The mineralization percentage was 82 %, 72 %, 40 % and 15 %, for each of the four cycles, as

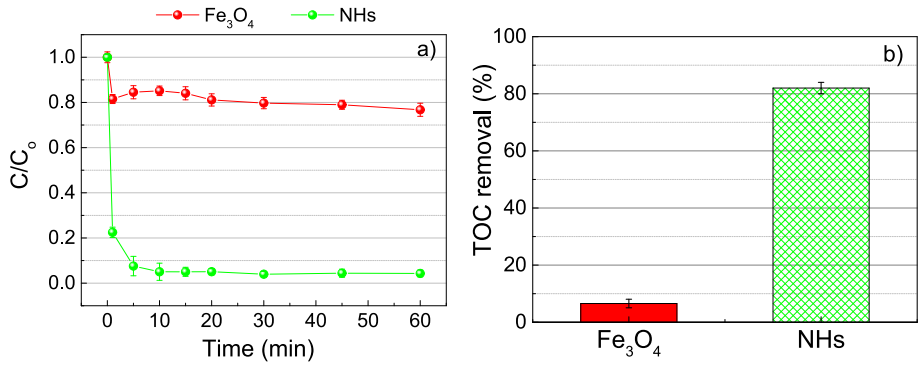

Fig. 5. a) UV–vis spectral changes for TCY discoloration with 1.0 g/L of catalyst and 0.5 mM of SPS at pH 6. b) TOC removal efficiencies obtained for the same experiment show in a) at time 1 h.

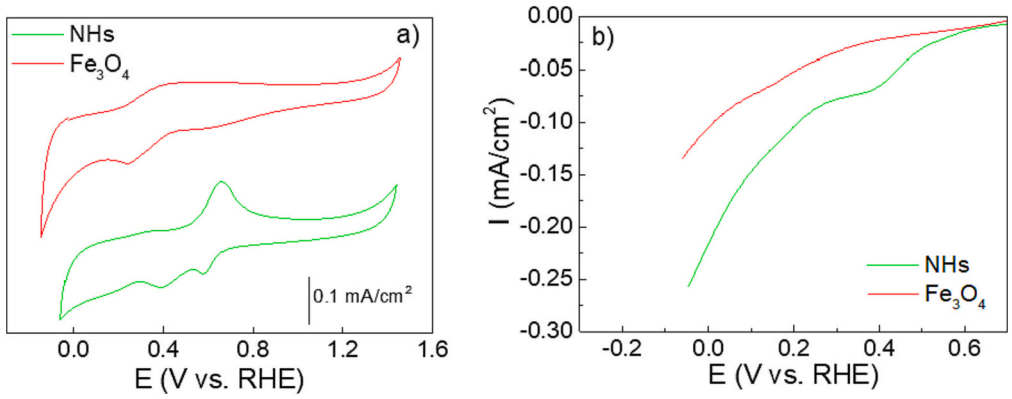

Fig. 6. a) Cyclic voltammetry of Fe_3O_4 and NHs recorded at 5 mV/s in pH 6 N_2 saturated solution. b) Polarization curves of Fe_3O_4 and NHs recorded at 5 mV/s in pH 6, 0.5 mM of SPS, N_2 saturated solution.

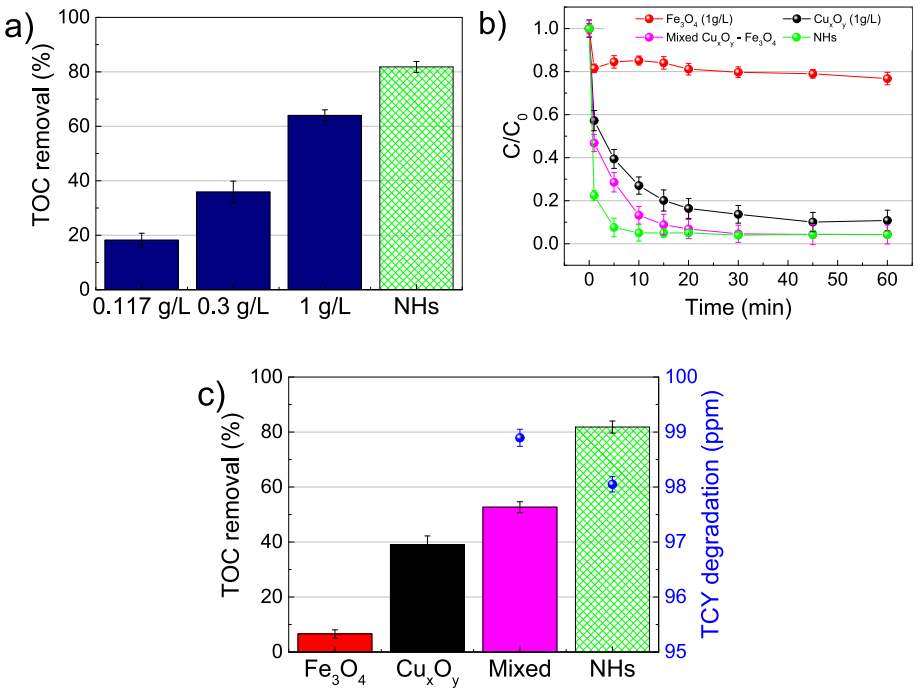

Fig. 7. a) TOC removal efficiencies obtained with commercial Cu_2O sample at different concentrations. b) UV–vis spectral changes for TCY degradation with 1.0 g/L of magnetite, 1.0 g/L electrochemical Cu_xO_y, 1.0 g/L sample of mixed (Cu_xO_y:magnetite) in proportion (0.117:0.883) and 1.0 g/L of NHs. (c) Target TCY degradation measured by HPLC for 1 h of experiment of mixed and NHs samples. TOC degradation efficiency of different catalyst (magnetite, electrochemical Cu_xO_y, mixed magnetite: Cu_xO_y and NHs).

shown in Fig. 8b. The reusability test showed an improved capacity of the catalyst to be reused in comparison with the $Cu/CuFe_2O_4$ catalyst proposed by [27], where at pH 7 in the second run, the efficiency was drastically reduced mainly due to the higher Cu leaching during the first run at this pH (100 mg/L). However, in the case of CuO particles encapsulated in a polyhedral carbon framework, the degradation rate diminished between the third and fifth runs, possibly caused by the adsorption of by-products on the catalyst active sites or by the leaching of copper [28].

It is evident, that after the oxidation process some catalyst leaching might appear by the consumption of SPS in the solution after each cycle, according to the mineralization reduction.

To further explore this hypothesis, the metal ion leaching after each cycle was also explored, Fig. 8c. The copper leaching from the nanohybrid structure has been more pronounced than iron loss. This evidence might result by the fact that the cuprite phase is non-magnetic and, therefore can stabilize eventually in aqueous media owing to their nanosized regimen making it impossible to collect them by centrifugation. Such particles may have subsequently been degraded in the acid digestion for ICP analysis; hence, the measured concentration is not exclusively of Cu ions in the solution and the Cu content might be overestimated. The weight content of Cu present in the NHs structure measured by ICP and referred to the total weight of the sample treated, is initially 17.8 %, followed by the values of 14.2 %, 10.6 %, 7.8 % and 3.8 % after successive degradation cycles. It seems evident that the substantial decrease in Cu concentration occurred throughout several runs compromised the catalyst reusability.

3.3. XPS characterization of the NHs after the degradation tests

After the degradation test, the surface composition of the NHs samples was characterized by XPS analysis and compared with the as-synthetized NHs. The atomic concentration (% at) after the AOPs, Ads + AOPs and the AOPs 4th run are summarized in Table 2.

As can be observed, the 3p and 2p intensity ratios are different in the as-synthetized NHs, and after the 1 step AOPs and Ads-AOPs tests, indicating that the enrichment of copper on the outer layer of the NHs remains during the first degradation tests. However, it is also worth mentioning that the analysis of the 3p and 2p core levels for the NHs-AOPs (4th run) sample provide the same value for both Cu/Fe ratios

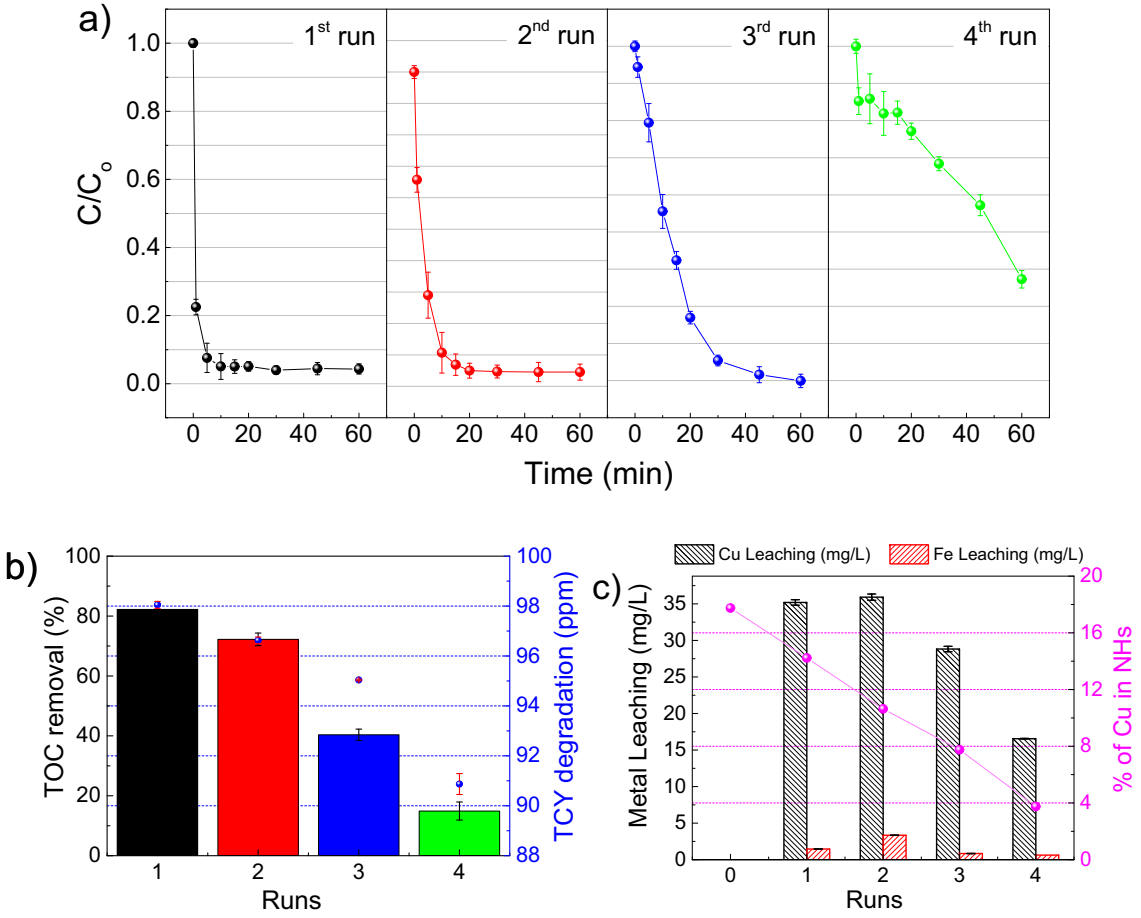

Fig. 8. (a) UV–vis spectral changes for TCY degradation with NHs cycling runs. (b) Target TCY degradation measured by HPLC (dots) and TOC removal efficiency (bars), both at 1 h of experiment after each run. (c) Metal ion leaching (bars) and weight percentage of Cu ions present in NHs measured by ICP after each cycle. Unless otherwise stated, the reaction conditions are based on: [TCY] = 100 ppm, [catalyst] = 1.0 g/L, T = 25 °C, [SPS] = 0.5 mM, time = 1 h, pH = 6.

Table 2
Relative percentage of elemental content obtained by XPS analysis, and Cu/Fe atomic ratio determined from 2p and 3p core levels emission, respectively.

Sample	Cu (2p/ 3p)	Fe (2p/ 3p)	C	O	N	Cu/Fe (2p)	Cu/Fe (3p)
NHs	6.4/ 5.7	4.9/ 5.8	55.0/ 54.9	33.7/ 33.6	–	1.30	0.98
NHs — AOPs	7.2/ 6.3	5.0/ 6.4	48.0/ 47.7	37.8/ 37.6	2.0/ 2.0	1.43	0.98
NHs — Ads + AOPs	2.4/ 2.8	1.8/ 2.9	68.1/ 67.0	27.1/ 26.7	0.6/ 0.6	1.33	0.97
NHs — AOPs (4th run)	0.7/ 1.1	1.9/ 3.3	69.7/ 68.7	26.5/ 26.0	1.2/ 1.2	0.37	0.37

so that relative total content of copper and iron is kept constant. Then, at this stage (4th run), the NHs can be considered as a uniform system according to XPS depth sensitivity. In the absence of Cu_2O shell, Cu^{2+} is present in the ferrite lattice in agreement with the XRD results for the spinel structure (Fig. S6), where a unique phase of Fd-3m:227 spatial group is observed.

As previously mentioned, XPS is particularly sensitive to the species present on the surface of the NHs, which is actually where the reaction takes place and can be an ideal technique to investigate the deactivation of the catalyst in the course of the reaction. The relative change in C, O and N content during the AOPs informs about the degradation mechanism. The N signal could be considered as a fingerprint of TCY degradation and adsorption on the surface of the NHs, and clearly appears upon the first step of AOPs and reaches its maximum intensity. After the adsorption-AOPs tests, the N signal is reduced due to the partial coverage of the NHs surface with high amount of OH groups, which produces a certain passivation effect. The last reaction step (4th) also shows a reduced N signal which explains the loss of catalytic activity of the NHs after the degradation results (Table 2).

At this point, further analysis of the corresponding C 1s and O 1s spectra are needed to study the progress of the reaction. Fig. 9, show the deconvolution analysis of the C 1s and O 1s spectra for the fresh NHs, NHs-AOPs and NHs-AOPs (4th run) samples. C 1s and O 1s fitting results are summarized in Table S3. C 1s has been decomposed into several components ascribed to the different chemical environment as C—C, C—OH/C—O, C═O, and O—C═O ordered from low to high binding energy values, respectively, in accordance with their respective energy shift values reported [49]. Analogously, O 1s has been fitted with three peaks attributed to lattice oxygen (O_L) bound to the metal cation in the catalyst (Cu, Fe-oxides), adsorbed surface oxygen including mainly oxygen species of hydroxyl groups, and water molecules and carbon-oxygen species adsorbed on the surface. O_L component has a strong signal for the fresh NHs sample due to the contribution of O bonding in the ferrite and cuprite lattices, which is difficult to be resolver individually. This component decreases in intensity in NHs-AOPs (4th run) due to the progressive release of Cu and the simultaneous adsorption of hydroxyl groups on the NHs surface, which agrees with the increment shown in the C 1s signal of carbon species bonded in the form of hydroxyl-carbonyl groups. Equivalent results are obtained for NHs-Ads + AOPs sample (not shown). The similarities of the C 1s and O 1s spectra

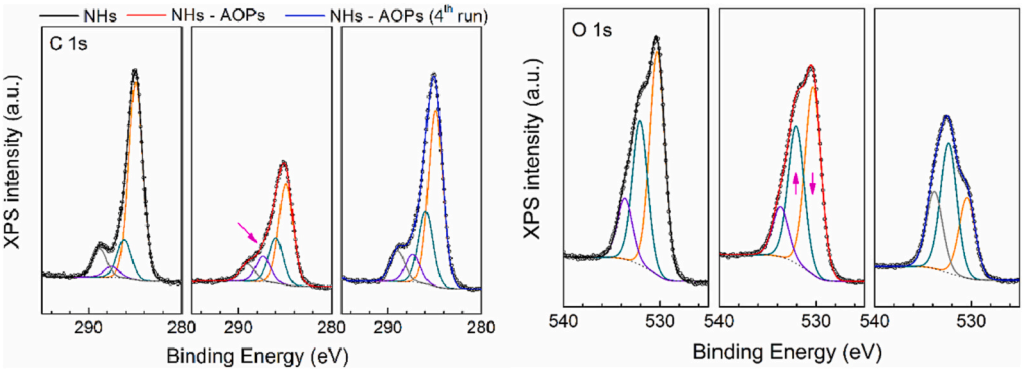

Fig. 9. Deconvolution analysis of the C 1s and O 1s spectra for the fresh NHs, NHs-AOPs and NHs-AOPs (4th run) samples.

(related to the deposition of oxidized carbonaceous species and OH groups derived from the adsorption stage and the 4th consecutive reuse of the NHs) might suggest a comparable catalytic behavior. However, it is important to remark on the very different relative surface content of Cu and Fe, which affect the efficiency of the TCY degradation process. In the case of NHs-Ads + AOPs reaction sample, NHs are able to preserve the high elimination efficiency with C/C_0 ratio very similar to that observed in NHs-AOPs, although limited by the TCY adsorption step and the consequent activation delay. On the contrary, in the case of NHs-AOPs (4th run) the reduced catalytic activity might be consequence of 1) the absence of the single Cu-oxide layer discussed in base of the Cu 2p/3p sensitive depth conditions and 2) the passivation of the outermost layer mainly covered by C—O species and OH groups (as already discussed).

Overall, we infer that the high efficiency of NHs is ascribed not only to the existence of Fe and Cu but also to the Cu^+ leaching in solution. Thus, the probable mechanism of the catalytic performance of tetracycline degradation is proposed in Fig. 10. In parentheses is depicted the equation proposed in the introduction which refers each process. The persulphate activation by Cu^+ and Fe^{2+} cations present in the catalyst surface, to generate $SO_4^{\bullet-}$, process (2 and 4). Also, the Cu^+ in solution behaves the process 4. The redox coupling Fe/Cu (process 5). The reaction of $SO_4^{\bullet-}$ in water to promotes the $OH^\bullet$ radicals generation, which are less reactive than $SO_4^{\bullet-}$. Finally, $SO_4^{\bullet-}$ and $OH^\bullet$ radicals react in Eq. 7 to degrade TCY in intermediates and $CO_2 + H_2O$.

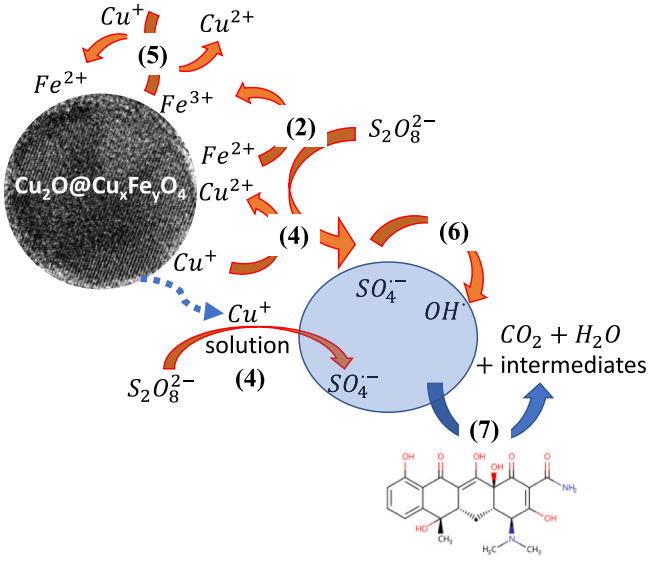

Fig. 10. Proposed advance oxidation process mechanism for the degradation of Tetracycline by $Cu_2O@Cu_xFe_yO_4$ nanohybrid and persulfate.

4. Conclusions

It is the first time shown that the electrochemical route can generates a catalyst (NHs) consisting of cuprite as a shell and non-stoichiometric spinel copper ferrite. This catalyst is able to reduce the concentration of tetracycline from the initial concentration, 100 ppm, up to 1 ppm in about 10 min reducing the total carbon content to 17.3 % in 1 h, with one of the lowest persulfate doses reported. The presence of Cu and Fe atoms at the surface provided catalyst with new properties, yielding great TCY degradation in one 1 h. In addition, the progressive release of Cu atoms from Cu-oxide NHs shell and their dilution into the medium has its own contribution. Complementary studies performed with catalyst consisted of a surface composition of Fe^{3+}/Fe^{2+} (Fe_3O_4), Cu^+ (Cu_2O), $Cu/Cu^+/Cu^{2+}$ (Cu_xO_y) and the catalyst mixture of Fe and Cu oxidation states (Fe_3O_4:Cu_xO_y) at the same experimental conditions shown poorer degradations yields. The catalyst loss its efficiency from 3rd cycle and onwards, because of the loss of Cu-shell with the consecutive runs and the adsorption of by-products or initial TCY which hinders the catalyst active sites, demonstrated by the reduction of the O_L component and the increment of C 1s signal of carbon species bonded in the form of hydroxyl-carbonyl groups in the XPS analysis. It has also been established that it is unnecessary to reach a steady state of adsorption before performing the degradation since the TOC removal, in this case, is worse than those obtained in a single degradation step, which is also time shorten.

Declaration of competing interest

The authors declare that they have no known competing financial interests or personal relationships that could have appeared to influence the work reported in this paper.

Data availability

Data will be made available on request.

Acknowledgments

This research was funded by the Madrid Government (Comunidad de Madrid-Spain) under the Multiannual Agreement with Universidad Autónoma de Madrid in the line of action encouraging youth research doctors, in the context of the V PRICIT (Regional Programme of Research and Technological Innovation) (SI1-PJI-2019-00366) and by the Spanish Ministry of Science and Innovation under project PID2021-123431OB-I00. FJP acknowledges financial support from Grant PID2021-126169OB-I00 funded by MCIN/AEI/10.13039/501100011033 and by "ERDF A way of making Europe". The authors would like to acknowledge to L. Gutierrez and the Advanced Microscopy Laboratory

(INA-Universidad de Zaragoza) for access to their instrumentation and expertise.

Appendix A. Supplementary data

Supplementary data to this article can be found online at https://doi.org/10.1016/j.jwpe.2023.103549.

References

[1] T.H. Grossman, Tetracycline antibiotics and resistance, Cold Spring Harb. Perspect. Med. 6 (2016), a025387, https://doi.org/10.1101/cshperspect.a025387.

[2] R. Daghrir, P. Drogui, Tetracycline antibiotics in the environment: a review, Environ. Chem. Lett. 11 (2013) 209–227, https://doi.org/10.1007/s10311-013-0404-8.

[3] K. Ji, S. Kim, S. Han, J. Seo, S. Lee, Y. Park, K. Choi, Y.-L. Kho, P.-G. Kim, J. Park, K. Choi, Risk assessment of chlortetracycline, oxytetracycline, sulfamethazine, sulfathiazole, and erythromycin in aquatic environment: are the current environmental concentrations safe? Ecotoxicology 21 (2012) 2031–2050, https://doi.org/10.1007/s10646-012-0956-6.

[4] D. Xu, Y. Xiao, H. Pan, Y. Mei, Toxic effects of tetracycline and its degradation products on freshwater green algae, Ecotoxicol. Environ. Saf. 174 (2019) 43–47, https://doi.org/10.1016/j.ecoenv.2019.02.063.

[5] M. Harnisz, E. Korzeniewska, I. Gołaś, The impact of a freshwater fish farm on the community of tetracycline-resistant bacteria and the structure of tetracycline resistance genes in river water, Chemosphere 128 (2015) 134–141, https://doi.org/10.1016/j.chemosphere.2015.01.035.

[6] J. Wang, L. Chu, L. Wojnárovits, E. Takács, Occurrence and fate of antibiotics, antibiotic resistant genes (ARGs) and antibiotic resistant bacteria (ARB) in municipal wastewater treatment plant: an overview, Sci. Total Environ. 744 (2020), 140997, https://doi.org/10.1016/j.scitotenv.2020.140997.

[7] R.K. Manoharan, F. Ishaque, Y.-H. Ahn, Fate of antibiotic resistant genes in wastewater environments and treatment strategies - a review, Chemosphere 298 (2022), 134671, https://doi.org/10.1016/j.chemosphere.2022.134671.

[8] D. Kanakaraju, B.D. Glass, M. Oelgemöller, Advanced oxidation process-mediated removal of pharmaceuticals from water: a review, J. Environ. Manag. 219 (2018) 189–207, https://doi.org/10.1016/j.jenvman.2018.04.103.

[9] C. Dong, W. Fang, Q. Yi, J. Zhang, A comprehensive review on reactive oxygen species (ROS) in advanced oxidation processes (AOPs), Chemosphere 308 (2022), 136205, https://doi.org/10.1016/j.chemosphere.2022.136205.

[10] J. Lee, U. von Gunten, J.-H. Kim, Persulfate-based advanced oxidation: critical assessment of opportunities and roadblocks, Environ. Sci. Technol. 54 (2020) 3064–3081, https://doi.org/10.1021/acs.est.9b07082.

[11] L.W. Matzek, K.E. Carter, Activated persulfate for organic chemical degradation: a review, Chemosphere 151 (2016) 178–188, https://doi.org/10.1016/j.chemosphere.2016.02.055.

[12] C.A.G. Bezerra, G.G. Bessegato, V.Del Colle, G. Tremiliosi-Filho, J.P.T.da S. Santos, C.L. de Paiva e Silva Zanta, Photo- and electro-oxidation of tetracycline hydrochloride on self-doped titanium dioxide nanotubes modified by Pt sub-monolayers, Electrochim. Acta 404 (2022) 139712, https://doi.org/10.1016/j.electacta.2021.139712.

[13] L. Hou, L. Wang, S. Royer, H. Zhang, Ultrasound-assisted heterogeneous Fenton-like degradation of tetracycline over a magnetite catalyst, J. Hazard. Mater. 302 (2016) 458–467, https://doi.org/10.1016/j.jhazmat.2015.09.033.

[14] S.O. Ganiyu, M. Zhou, C.A. Martínez-Huitle, Heterogeneous electro-Fenton and photoelectro-Fenton processes: a critical review of fundamental principles and application for water/wastewater treatment, Appl. Catal. B Environ. 235 (2018) 103–129, https://doi.org/10.1016/j.apcatb.2018.04.044.

[15] S. Tang, M. Zhao, D. Yuan, X. Li, Z. Wang, X. Zhang, T. Jiao, J. Ke, Fe3O4 nanoparticles three-dimensional electro-peroxydisulfate for improving tetracycline degradation, Chemosphere 268 (2021), 129315, https://doi.org/10.1016/j.chemosphere.2020.129315.

[16] A.A. Oladipo, M.A. Abureesh, M. Gazi, Bifunctional composite from spent “Cyprus coffee” for tetracycline removal and phenol degradation: solar-Fenton process and artificial neural network, Int. J. Biol. Macromol. 90 (2016) 89–99, https://doi.org/10.1016/j.ijbiomac.2015.08.054.

[17] A. Jonidi Jafari, B. Kakavandi, N. Jaafarzadeh, R. Rezaei Kalantary, M. Ahmadi, A. Akbar Babaei, Fenton-like catalytic oxidation of tetracycline by AC@Fe3O4 as a heterogeneous persulfate activator: adsorption and degradation studies, J. Ind. Eng. Chem. 45 (2017) 323–333, https://doi.org/10.1016/j.jiec.2016.09.044.

[18] S. Wang, J. Wang, Trimethoprim degradation by Fenton and Fe(II)-activated persulfate processes, Chemosphere 191 (2018) 97–105, https://doi.org/10.1016/j.chemosphere.2017.10.040.

[19] H. Zhang, J. Liu, C. Ou, J. Faheem, H. Shen, Z. Yu, W. Jiao, X. Han, J. Sun, L. Wang Li, Reuse of Fenton sludge as an iron source for NiFe2O4 synthesis and its application in the Fenton-based process, J. Environ. Sci. 53 (2017) 1–8, https://doi.org/10.1016/j.jes.2016.05.010.

[20] H. Qin, H. Cheng, H. Li, Y. Wang, Degradation of ofloxacin, amoxicillin and tetracycline antibiotics using magnetic core–shell MnFe2O4@C-NH2 as a heterogeneous Fenton catalyst, Chem. Eng. J. 396 (2020), 125304, https://doi.org/10.1016/j.cej.2020.125304.

[21] G. Ayoub, A. Ghauch, Assessment of bimetallic and trimetallic iron-based systems for persulfate activation: application to sulfamethoxazole degradation, Chem. Eng. J. 256 (2014) 280–292, https://doi.org/10.1016/j.cej.2014.07.002.

[22] S. Wacławek, H.V. Lutze, K. Grübel, V.V.T. Padil, M. Černík, D.D. Dionysiou, Chemistry of persulfates in water and wastewater treatment: a review, Chem. Eng. J. 330 (2017) 44–62, https://doi.org/10.1016/j.cej.2017.07.132.

[23] M. Shen, Z. Huang, X. Luo, Y. Ma, C. Chen, X. Chen, L. Cui, Activation of persulfate for tetracycline degradation using the catalyst regenerated from Fenton sludge containing heavy metal: synergistic effect of Cu for catalysis, Chem. Eng. J. 396 (2020), 125238, https://doi.org/10.1016/j.cej.2020.125238.

[24] A. Idrees, A. Shan, M. Danish, W.Q. Zaman, A. Mohsin, Z. Abbas, J. Huang, T. Shahzad, Y. Sun, Z. Xu, S. Lyu, Influence of preparation method on copper ferrite characteristics for the efficient degradation of trichloroethylene in persulfate activated system, J. Environ. Chem. Eng. 9 (2021), 106044, https://doi.org/10.1016/j.jece.2021.106044.

[25] F. Chen, S. Xie, X. Huang, X. Qiu, Ionothermal synthesis of Fe3O4 magnetic nanoparticles as efficient heterogeneous Fenton-like catalysts for degradation of organic pollutants with H2O2, J. Hazard. Mater. 322 (2017) 152–162, https://doi.org/10.1016/j.jhazmat.2016.02.073.

[26] X. Li, K. Cui, Z. Guo, T. Yang, Y. Cao, Y. Xiang, H. Chen, M. Xi, Heterogeneous Fenton-like degradation of tetracyclines using porous magnetic chitosan microspheres as an efficient catalyst compared with two preparation methods, Chem. Eng. J. 379 (2020), 122324, https://doi.org/10.1016/j.cej.2019.122324.

[27] Z. Li, C. Guo, J. Lyu, Z. Hu, M. Ge, Tetracycline degradation by persulfate activated with magnetic Cu/CuFe2O4 composite: efficiency, stability, mechanism and degradation pathway, J. Hazard. Mater. 373 (2019) 85–96, https://doi.org/10.1016/j.jhazmat.2019.03.075.

[28] D. Yang, P. Hong, Y. Hu, Y. Li, C. Wang, J. He, B. Sun, S. Zhu, L. Kong, J. Liu, Carbon framework-encapsulated copper oxide particles to activate peroxymonosulfate for the efficient degradation of tetracycline, Appl. Surf. Sci. 552 (2021), 149424, https://doi.org/10.1016/j.apsusc.2021.149424.

[29] G. Zhu, X. Yu, F. Xie, W. Feng, Ultraviolet light assisted heterogeneous Fenton degradation of tetracycline based on polyhedral Fe3O4 nanoparticles with exposed high-energy 110 facets, Appl. Surf. Sci. 485 (2019) 496–505, https://doi.org/10.1016/j.apsusc.2019.04.239.

[30] P. Lozano, Ivan; lopez, Claudia; menendez, nieves; Casillas, norberto; herrasti, design, construction and evaluation of a 3D printed electrochemical flow cell for the synthesis of magnetite nanoparticles, J. Electrochem. Soc. 165 (2018) H688–H697.

[31] E. Mazario, M.P. Morales, R. Galindo, P. Herrasti, N. Menendez, Influence of the temperature in the electrochemical synthesis of cobalt ferrites nanoparticles, J. Alloys Compd. 536 (2012), https://doi.org/10.1016/j.jallcom.2011.10.073.

[32] F.L. Rivera, J. Sanchez-Marcos, N. Menendez, P. Herrasti, E. Mazario, Tunneling the size of iron oxide NPs using different alcohols and proportions water-alcohol, Adv. Nano Res. 8 (2020) 95–102, https://doi.org/10.12989/anr.2020.8.2.095.

[33] B.V. PANalytical, X’pert Highscore Plus, X’Pert HighScore Plus, Lelyweg, Almelo, the Netherlands 2, 2002.

[34] J. Rodríguez-Carvajal, Recent advances in magnetic structure determination by neutron powder diffraction, Phys. B Condens. Matter 192 (1993) 55–69.

[35] D.G. Calatayud, T. Jardiel, M. Peiteado, F. Illas, E. Giamello, F.J. Palomares, D. Fernández-Hevia, A.C. Caballero, Synthesis and characterization of blue faceted anatase nanoparticles through extensive fluorine lattice doping, J. Phys. Chem. C 119 (2015) 21243–21250, https://doi.org/10.1021/acs.jpcc.5b06923.

[36] J. Calvo-de la Rosa, M. Segarra Rubí, Influence of the synthesis route in obtaining the cubic or tetragonal copper ferrite phases, Inorg. Chem. 59 (2020) 8775–8788, https://doi.org/10.1021/acs.inorgchem.0c00416.

[37] R.S. Yadav, J. Havlica, J. Masilko, L. Kalina, J. Wasserbauer, M. Hajdúchová, V. Enev, I. Kuřitka, Z. Kožáková, Cation migration-induced crystal phase transformation in copper ferrite nanoparticles and their magnetic property, J. Supercond. Nov. Magn. 29 (2016) 759–769, https://doi.org/10.1007/s10948-015-3339-4.

[38] Á. Gallo-Cordova, A. Espinosa, A. Serrano, L. Gutiérrez, N. Menéndez, M. Del Puerto Morales, E. Mazarió, New insights into the structural analysis of maghemite and (MFe2O4, M = co, Zn) ferrite nanoparticles synthesized by a microwave-assisted polyol process, Mater. Chem. Front. 4 (2020), https://doi.org/10.1039/D0QM00460J.

[39] M.C. Biesinger, B.P. Payne, A.P. Grosvenor, L.W.M. Lau, A.R. Gerson, R.S.C. Smart, Resolving surface chemical states in XPS analysis of first row transition metals, oxides and hydroxides: Cr, Mn, Fe, Co and Ni, Appl. Surf. Sci. 257 (2011) 2717–2730, https://doi.org/10.1016/j.apsusc.2010.10.051.

[40] M.C. Biesinger, Advanced analysis of copper X-ray photoelectron spectra, Surf. Interface Anal. 49 (2017) 1325–1334, https://doi.org/10.1002/sia.6239.

[41] C. Gu, K.G. Karthikeyan, Interaction of tetracycline with aluminum and iron hydrous oxides, Environ. Sci. Technol. 39 (2005) 2660–2667, https://doi.org/10.1021/es048603o.

[42] Y. Yang, X. Hu, Y. Zhao, L. Cui, Z. Huang, J. Long, J. Xu, J. Deng, C. Wu, W. Liao, Decontamination of tetracycline by thiourea-dioxide–reduced magnetic graphene oxide: effects of pH, ionic strength, and humic acid concentration, J. Colloid Interface Sci. 495 (2017) 68–77, https://doi.org/10.1016/j.jcis.2017.01.075.

[43] M. Yuan, C. Li, B. Zhang, J. Wang, J. Zhu, J. Ji, Y. Ma, A mild and one-pot method to activate lignin-derived biomass by using boric acid for aqueous tetracycline antibiotics removal in water, Chemosphere 280 (2021), 130877, https://doi.org/10.1016/j.chemosphere.2021.130877.

[44] B. Huang, Y. Liu, B. Li, S. Liu, G. Zeng, Z. Zeng, X. Wang, Q. Ning, B. Zheng, C. Yang, Effect of Cu(II) ions on the enhancement of tetracycline adsorption by

Fe3O4@SiO2-Chitosan/graphene oxide nanocomposite, Carbohydr. Polym. 157 (2017) 576–585, https://doi.org/10.1016/j.carbpol.2016.10.025.
[45] C. Liang, Z.-S. Wang, C.J. Bruell, Influence of pH on persulfate oxidation of TCE at ambient temperatures, Chemosphere 66 (2007) 106–113, https://doi.org/10.1016/j.chemosphere.2006.05.026.
[46] D.A. House, Kinetics and mechanism of oxidations by peroxydisulfate, Chem. Rev. 62 (1962) 185–203, https://doi.org/10.1021/cr60217a001.
[47] J.J.P. Roberts, J.A. Westgard, L.M. Cooper, R.W. Murray, Solution voltammetry of 4 nm magnetite iron oxide nanoparticles, J. Am. Chem. Soc. 136 (2014) 10783–10789, https://doi.org/10.1021/ja505562p.
[48] S. Mirehbar, S. Fernandez-Velayos, E. Mazario, N. Menendez, P. Herrasti, F. J. Recio, I. Sires, Evidence of cathodic peroxydisulfate activation via electrochemical reduction at Fe(II) sites of magnetite-decorated porous carbon: application to dye degradation in water, J. Electroanal. Chem. 902 (2021), https://doi.org/10.1016/j.jelechem.2021.115807.
[49] F. Della Pelle, R. Di Battista, L. Vázquez, F.J. Palomares, M. Del Carlo, M. Sergi, D. Compagnone, A. Escarpa, Press-transferred carbon black nanoparticles for class-selective antioxidant electrochemical detection, Appl. Mater. Today 9 (2017) 29–36, https://doi.org/10.1016/j.apmt.2017.04.012.